Optimized Choice of Light Incidence Angles for the Determination of Optical Constants from Strongly Absorbing Thin Solid Films in a Narrow Spectral Range

Steffen Wilbrandt and Olaf Stenzel *

Posted Date: 1 April 2026

doi: 10.20944/preprints202604.0015.v1

Keywords: optical constants; refractive index; extinction coefficient; reflectance; transmittance; ellipsometry; absorption

 doi:10.20944/preprints202604.0015.v1

Article

Optimized Choice of Light Incidence Angles for the Determination of Optical Constants from Strongly Absorbing Thin Solid Films in a Narrow Spectral Range

Steffen Wilbrandt [1] and Olaf Stenzel [1,2,*]

[1] Fraunhofer Institute for Applied Optics and Precision Engineering, Albert-Einstein-Str. 7, 07745 Jena, Germany

[2] Institute of Applied Physics, Friedrich-Schiller-University, Max-Wien-Platz 1, 07743 Jena, Germany

* Correspondence: olaf.stenzel@iof.fraunhofer.de; Tel.: +49-3641-807348

Abstract

The determination of the linear optical constants of solids is an important part of solid state optical characterization. Reflection spectroscopy and ellipsometry of surfaces or thin solid films represent established techniques to access those optical constants, however, they may suffer from an ambiguity of the obtained optical constants. We discuss methods for identifying the physically meaningful solution from the solution multiplicity, making use of a proper combination of independent measurements. Elaborating contours of constant reflectance (iso-reflectance curves) facilitates reliable identification of correct optical constants. A numerical criterion is further provided to select suitable combinations of measurements. The procedure is demonstrated in application to simulated spectra of a Nb_2O_5 film in the spectral region where the onset of the fundamental absorption edge is observed.

Keywords: optical constants; refractive index; extinction coefficient; reflectance; transmittance; ellipsometry; absorption

1. Introduction

Determining the optical constants of solid materials by means of optical spectroscopy of solid surfaces or thin solid films is a recurring task in the optical spectroscopy of solids. Contrary to what the name "optical constants" suggests, they are not only a material-specific property but are also significantly influenced by the real structure of the investigated solid material. Particularly in the case of thin solid films, the latter depends crucially on the selected coating process and the associated distributions of energy and momentum of the film-forming particles (e.g. inert and reactive gas inlets [1–5]).

In optical coating design, the optical constants of the corresponding materials are assumed to be known and only the layer sequence and their thicknesses are determined. The process-specific optical constants are usually determined on suitable single layers using spectrophotometry or/and ellipsometry in terms of a reverse search procedure [6–10]. For dielectric layers in the transparency range, this is a routine task for which different methods have been established depending on the available measurement technology [11–16]. The characterization of such a single layer on a known (often transparent) substrate can already be performed in the frames of the model of a homogeneous thin solid film with smooth and parallel interfaces (Figure 1) by means of spectral transmission measurement and the use of a simple dispersion model (e.g., Cauchy or Sellmeier) [17].

 doi:10.20944/preprints202604.0015.v1

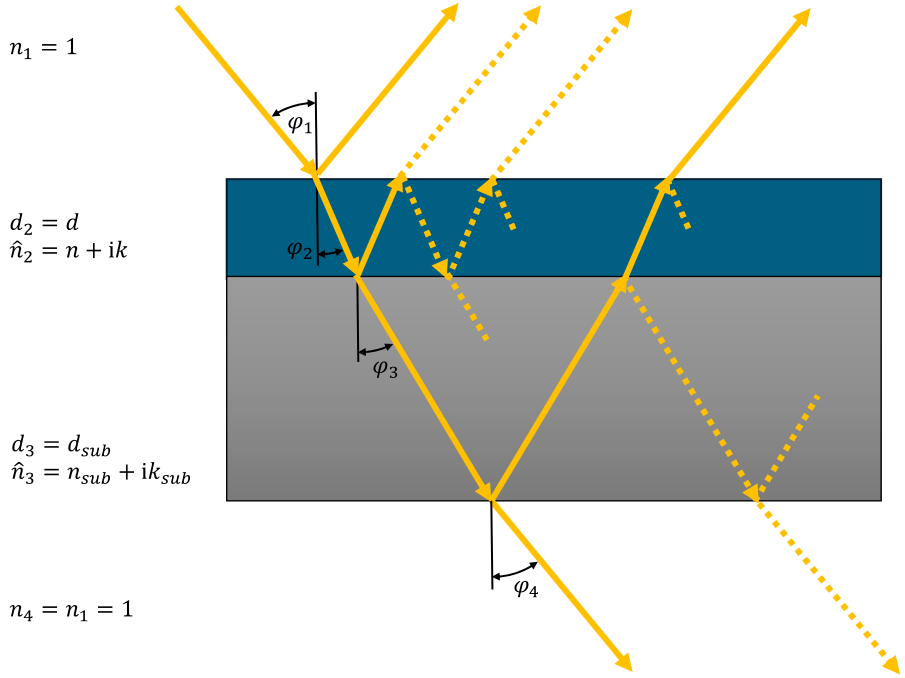

Figure 1. Model of a homogenous single layer (refractive index n, extinction coefficient k, thickness d, coherent light propagation) with smooth and parallel interfaces on a known substrate (refractive index n_{sub}, extinction coefficient k_{sub}, thickness d_{sub}, incoherent light propagation) with air as ambient medium at front and backside of the coating. Contributions of different light paths (yellow lines) and relevant angles are indicated. Thicknesses are not true to scale, because $d \ll d_{sub}$ is assumed. In absorbing materials, the propagation angles must be tackled as complex parameters.

By incorporating spectral reflectance data, a reliable characterization is also possible in spectral regions where weak absorption occurs. This simple approach fails when the absorption becomes so strong that the transmission signal practically disappears. This is the case for typical high-refractive index coating materials (TiO_2, Ta_2O_5, Nb_2O_5, ZrO_2, and HfO_2) in the ultraviolet spectral range at coating thicknesses that cause significant interference effects in the visible spectral range. Usually, this concerns coatings with an optical thickness of a few hundred nanometers. A particular problem is in the ambiguity of the obtained optical constants [18] and it occurs already in the absence of absorption, when spectrophotometry is used for single layer characterization on a substrate with a higher refractive index [19]. Therefore, additional information is required to determine the optical constants (refractive index n, extinction coefficient k) unambiguously.

This article focuses on the choice of optical measurements best suited for reducing ambiguity of the reverse search task when strong absorption occurs. This may be of relevance in the case of material characterization for solar absorber or solar cell applications. Also, the determination of optical constants at the fundamental absorption edge of dielectrics or semiconductors will be addressed this way. This will be illustrated using Nb_2O_5 and its optical constants published by Franta [20] as a model system. To eliminate non-physical solutions, the use of a Kramer-Kronig-consistent dispersion model is often favored [20,21]. Note that such models automatically provide access to anomalous dispersion, as evident for Nb_2O_5, anomalous dispersion can already be observed in the wavelength range up to 250 nm (wavenumber 40000 cm^{-1}, Figure 2). The wavenumber ν is related to the vacuum wavelength λ through $\nu = \lambda^{-1}$.

Since the fundamental problem of solution ambiguity already occurs in the model of homogeneous layers with smooth interfaces, it is sufficient to make these simplifying assumptions for its discussion.

 doi:10.20944/preprints202604.0015.v1

Note that the requirement of Kramers-Kronig consistency for eliminating non-physical dispersion solutions will lose efficiency when the investigated spectral range is too narrow. In this case, the elimination of non-physical solutions by a suitable combination of independent measurements may be the method of choice [22–29]. A comparative analysis of the accuracy of reflectance methods for determining the optical constants of highly absorbing films is provided in [30]. In the forthcoming, we will focus on this situation. Attention will be paid to the choice of angles of incidence. Emphasis will be placed on near-normal incidence as well as incidence angles in the region of the pseudo-Brewsters angle φ_B (which minimizes the surface reflectance at p-polarization [31,32]), as well as the second Brewsters angle φ_{B2} (which minimizes the ratio of surface reflectance's at p- and s-Polarization [33]). In the case of dielectric coatings at the absorption edge, the difference of both angles is commonly small [34]. Clearly, the knowledge of the pseudo-Brewster angle and corresponding reflectance for p polarization can be used for a direct determination of the optical constants [35–38].

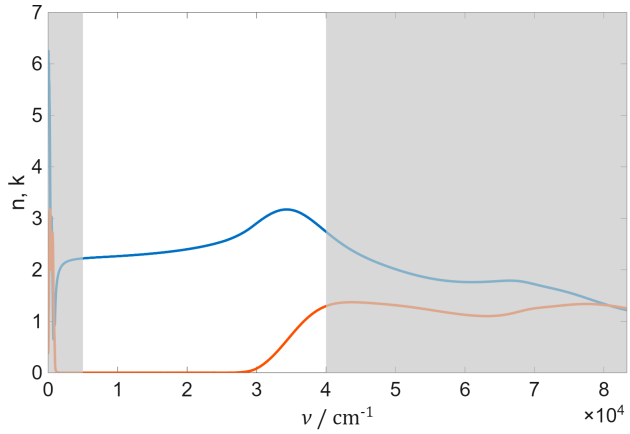

Figure 2. Optical constants n (blue line) and k (red line) of Nb_2O_5 [20], white background indicates spectral range addressed in this article.

The typical geometrical layer thickness of a highly refractive single layer for characterization in the UV/VIS/NIR spectral range is around 200 nm. The theoretical transmittance of such an Nb_2O_5 layer on a 1 mm thick quartz glass substrate is shown in Figure 3 (a). Several transmittance extrema can be observed in the transparency range, providing access to the optical thickness of the film [19,39]. At the same time, the refractive index can be determined making use of envelope methods [40]. In the wavenumber range above 35000 cm^{-1}, the transmission signal disappears almost completely. In fact, however, it is only very small and can still be reliably detected with a standard spectrophotometer. This is clearly visible in the logarithmic representation (Figure 3b). This form of representation is common, as, for example, the optical density is often specified for neutral density filters [41] instead of the transmittance. The following applies to the relationship between the two variables.

$$OD = -\lg T \tag{1}$$

The detectable optical density OD here is 6, which is significantly below the optical density of 8 specified by PerkinElmer for the Lambda 1050+ spectrophotometer [42]. Since this measurement is relatively easy to perform, it provides valuable information for characterization and will be further discussed later. If the available spectrophotometer is unable to detect the required optical density, the inclusion of an additional sample with a smaller layer thickness may be helpful. For a layer thickness of 50 nm, a significant transmission signal with approx. 0.027 is still available on a quartz glass substrate at 40000 cm^{-1}. However, it should be noted that deviating layer properties may occur in the growth zone (e.g., in the case of Ta_2O_5 [43]). In this case, the model of homogeneous, isotropic layers considered here cannot find application.

 doi:10.20944/preprints202604.0015.v1

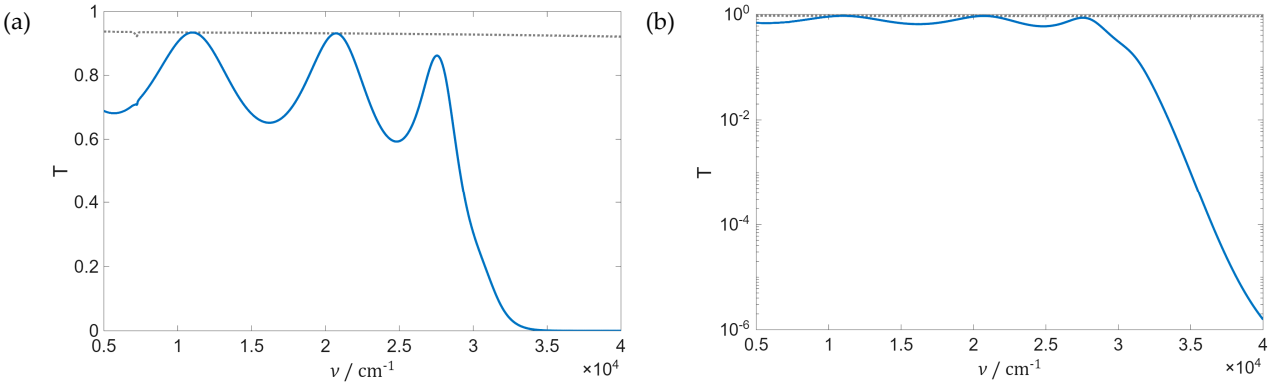

Figure 3. Linear (a) and logarithmic (b) scaled theoretical transmittance at normal incidence of the uncoated fused silica substrate (thickness 1mm, dotted line, optical constants from [20]) and with a 200 nm thick Nb_2O_5 single layer (solid line).

While the use of transmission measurements requires application of a transparent substrate, the choice of the substrate is almost irrelevant for the result of the reflection measurement of absorbing coatings. Accordingly, the reflection spectra for wave numbers above approx. 35000 cm^{-1} of the mentioned Nb_2O_5 film are practically identical for substrates made of quartz (optical constants from [44]) or silicon (optical constants from [45]), while they differ significantly for smaller wave numbers (Figure 4).

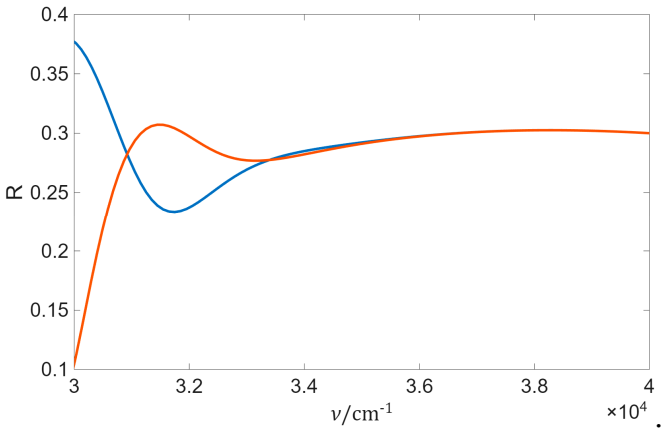

Figure 4. Normal incidence theoretical reflectance of a 200 nm thick Nb_2O_5 single layer (optical constants from [20]) on a fused silica (blue) and silicon (red) substrate (thickness 1mm, optical constants from [44,45]).

The use of a transparent substrate for characterization in the absorption edge region nevertheless provides access to potentially useful additional information, since the reflections measured from the front and back sides differ in lossy layer systems [46]. For the 200 nm thick Nb_2O_5 layer on a quartz glass substrate, the front- and backside reflectance's differ up to 0.1 (Figure 5).

 doi:10.20944/preprints202604.0015.v1

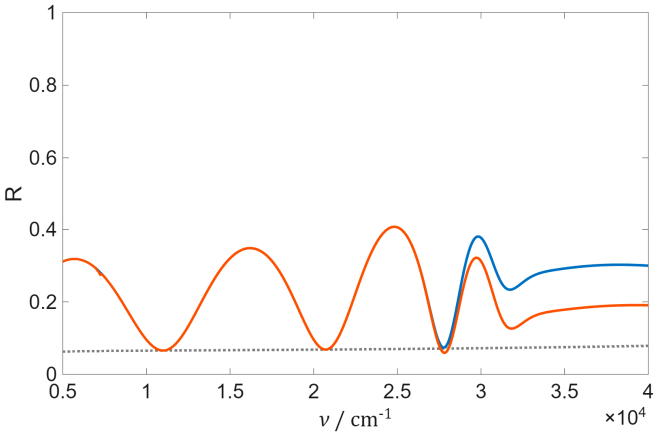

Figure 5. Normal incidence front and backside reflectance of a 200 nm thick Nb_2O_5 single layer on a fused silica substrate (thickness 1mm). Dotted line indicates normal incidence reflectance of the uncoated substrate.

For characterization using ellipsometry, measurements are usually taken in reflection at large angles of incidence. The ellipsometry quantities Ψ and Δ are derived from the ratio of the complex reflection coefficients $\hat{r}_s$ and $\hat{r}_p$ for s- and p-polarization, respectively.

$$\frac{\hat{r}_p}{\hat{r}_s} = \tan\Psi\, e^{i\Delta} \tag{2}$$

In a thin-film system, depolarization by the substrate back side poses an additional challenge [47]. Figure 6 shows the theoretical ellipsometry parameters for a 200 nm thick Nb_2O_5 single layer on both quartz and silicon substrates, with and without consideration of the substrate back side.

As already mentioned, spectra like shown in Figures 3 or 5 are accessible to optical constants determination by envelope methods [40]. The focus of our study is rather on the elaboration of spectra that lack interference pattern, like the reflection spectra in Figure 4. In this context, the term "narrow spectral range" denotes a spectral range, that

- does not include a relevant interference pattern of the thin film spectrum and
- is much too narrow to exhaust typical sum rules [48–50].

In the extreme case, that narrow spectral range degenerates to a single wavelength (or wavenumber) value, defining what is called a single-wavelength method [7,51,52]. Frequently, the examples discussed in this study will concern this extreme case.

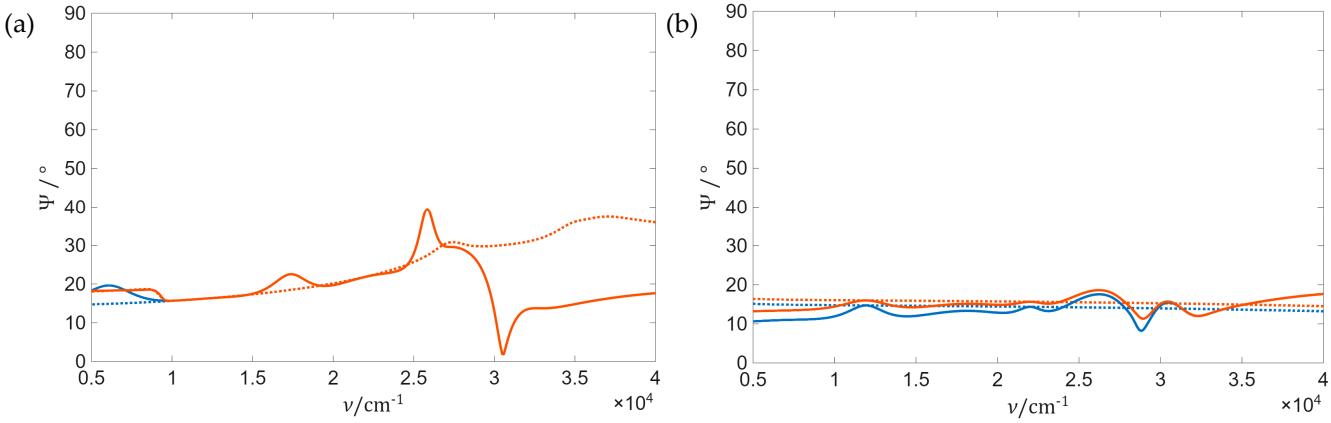

 doi:10.20944/preprints202604.0015.v1

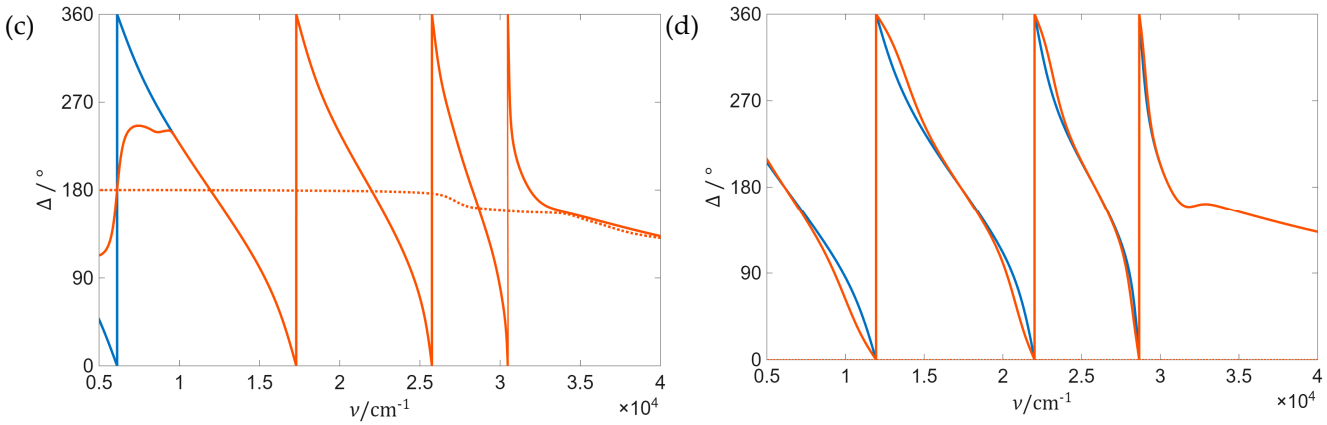

Figure 6. Ellipsometry measures Ψ and Δ at 65° angle of incidence of the uncoated substrate (dotted line, thickness 1mm, silicon in (a) and (c), fused silica in (b) and (d)) and with a 200 nm thick Nb_2O_5 single layer with (red) and without (blue) consideration of substrate backside.

2. Theoretical Aspects

Front reflectance R, backside reflectance BR, and transmittance T of the film system shown in Figure 1 can be calculated in terms of the following couple of equations:

$$R = |\hat{r}_{123}|^2 + \frac{|\hat{t}_{123}|^2|\hat{r}_{31}|^2|\hat{t}_{321}|^2 e^{-4\,Im\,\hat{\delta}_3}}{1 - |\hat{r}_{321}|^2|\hat{r}_{31}|^2 e^{-4\,Im\,\hat{\delta}_3}}$$

$$BR = |\hat{r}_{13}|^2 + \frac{|\hat{t}_{13}|^2|\hat{r}_{321}|^2|\hat{t}_{31}|^2 e^{-4\,Im\,\hat{\delta}_3}}{1 - |\hat{r}_{321}|^2|\hat{r}_{31}|^2 e^{-4\,Im\,\hat{\delta}_3}} \tag{3}$$

$$T = \frac{|\hat{t}_{123}|^2|\hat{t}_{31}|^2 e^{-2\,Im\,\hat{\delta}_3}}{1 - |\hat{r}_{321}|^2|\hat{r}_{31}|^2 e^{-4\,Im\,\hat{\delta}_3}}$$

with

$$\hat{r}_{ijk} = \frac{\hat{r}_{ij} + \hat{r}_{jk} e^{2i\hat{\delta}_j}}{1 + \hat{r}_{ij}\hat{r}_{jk} e^{2i\hat{\delta}_j}}$$

$$\hat{t}_{ijk} = \frac{\hat{t}_{ij}\hat{t}_{jk} e^{i\hat{\delta}_j}}{1 + \hat{r}_{ij}\hat{r}_{jk} e^{2i\hat{\delta}_j}} \tag{4}$$

and

$$\hat{\delta}_i = 2\pi\nu d_i \sqrt{\hat{n}_i^2 - n_1^2 \sin^2 \varphi_1} \tag{5}$$

The polarization dependence (s- or p-polarization) is hidden in the Fresnel's formulas (here written in the Mueller convention [53]):

$$\hat{r}_{ij}^s = \frac{\hat{n}_i \cos\varphi_i - \hat{n}_j \cos\varphi_j}{\hat{n}_i \cos\varphi_i + \hat{n}_j \cos\varphi_j}$$

$$\hat{r}_{ij}^p = \frac{\hat{n}_j \cos\varphi_i - \hat{n}_i \cos\varphi_j}{\hat{n}_j \cos\varphi_i + \hat{n}_i \cos\varphi_j} \tag{6}$$

$$\hat{t}_{ij}^s = \frac{2\hat{n}_i \cos\varphi_i}{\hat{n}_i \cos\varphi_i + \hat{n}_j \cos\varphi_j}$$

 doi:10.20944/preprints202604.0015.v1

$$\hat{t}_{ij}^{p} = \frac{2\hat{n}_i \cos\varphi_i}{\hat{n}_j \cos\varphi_i + \hat{n}_i \cos\varphi_j}$$

The theoretical spectra shown in Figures 3–5 have been calculated in terms of these equations.

If the film (material 2) absorption is sufficiently strong ($\pi\nu k_2 d_2 \gg 1$), simpler equations may find application. Then, the front side reflectance may be approximated by a single interface between a transparent medium with refractive index n_1 and an absorbing medium with refractive index n and extinction coefficient k, where the complex refractive index $\hat{n}$ is given by the relationship $\hat{n}_2 = \hat{n} = n + ik$.

The normal incidence front reflectance is then:

$$R = \frac{(n_1 - n)^2 + k^2}{(n_1 + n)^2 + k^2} = 1 - \frac{4n_1 n}{(n_1 + n)^2 + k^2} \tag{7}$$

By simple transformation, the equation can be converted into the common form describing a circle in the n-k-plane [31,54]:

$$\left(n - n_1 \frac{1+R}{1-R}\right)^2 + K^2 = \left(2n_1 \frac{\sqrt{R}}{1-R}\right)^2 \tag{8}$$

Equation (8) has the meaning that the combinations of n- and k-values that correspond to a certain normal incidence reflectance of a strongly absorbing film are represented by circles in the n-k-plane. In the forthcoming, such type of curves (i.e. contours of constant reflectance [22,63]) will be called iso-reflectance curves.

For reflection from the front side, $n_1 = 1$ must be set, whereas for measurement from the back side, the substrate refractive index n_{sub} is relevant and $n_1 = n_{sub}$ applies (here a non-absorbing substrate is assumed). However, the interface of the substrate to air needs to be considered as well. This can easily be done and results in the following equation:

$$BR = 1 - \frac{4nn_{sub}}{n + k^2 + n^2 + n_{sub}^2(n+1)} \tag{9}$$

Again, this results in the equation of a circle in the n-k-plane:

$$\left[n - \left(\frac{2n_{sub}}{1-BR} - \frac{1+n_{sub}^2}{2}\right)\right]^2 + k^2 = \left[\frac{1}{2}\left(1 + n_{sub}^2 - \frac{4n_{sub}}{1-BR}\right)\right]^2 - n_{sub}^2 \tag{10}$$

Since both the normal incidence iso-reflectance curves for front and back side reflectance's of strongly absorbing films can be represented as circles in the n-k-plane, in this study, this form of representation is used. Other representations that use the real and imaginary parts of the dielectric function instead can be found in the literature, for example for contour lines of the pseudo-Brewster angle [31]. Similar contour-plots can be also found for other quantities [55–57].

Figure 7 exemplifies iso-reflectance curves for the R and BR using the thin-film model from Figure 1 (Equations (3)-(6) assuming normal incidence) as red lines. The calculations are performed for a 200 nm thick Nb_2O_5 layer (optical constants from [20], indicated by a black cross) on a 1 mm thick quartz glass substrate (optical constants from [44]) with air as the ambient medium for a wave number of 40000 cm^{-1} (wavelength 250 nm). The shape of the iso-reflectance curves according to (3)-(6) is much more complex than those according to (8) and (10) (large blue circle with indicated center by a small circle) described above. In the range of low extinction coefficients, there are several contours that differ in their refractive index. This multiplicity of possible n-k-pairs is a consequence of interference in the single layer coating and therefore only occurs when the extinction coefficient is sufficiently small [58]. In spectroscopy practice, they define a set of multiple solutions of the reverse task, when n and k are to be calculated from a measured reflectance. These potential but non-valid solutions can be ruled out by means of an additional transmission measurement. At larger extinction coefficients, the red iso-reflectance curve practically coincides with the circle predicted by (8) or (10) (blue curve).

 doi:10.20944/preprints202604.0015.v1

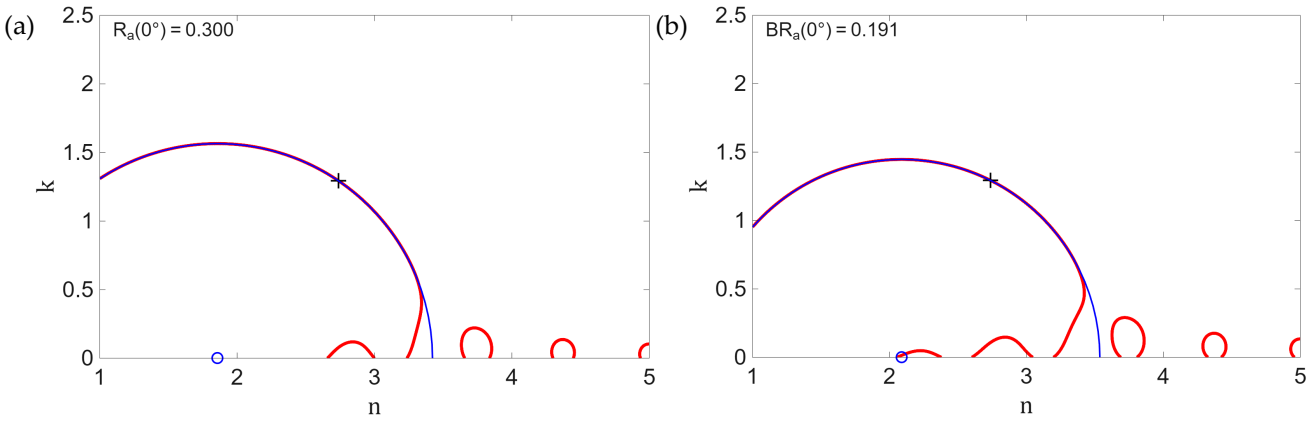

Figure 7. Normal incidence iso-reflectance plot (red line) for R (a) and BR (b); corresponding theoretical values are from a 200 nm Nb_2O_5 layer single layer coating on a 1 mm thick fused silica substrate at 40000cm^{-1}; blue lines: circles according to eqs. (8) and (10) with indicated center positions.

At oblique incidence, the expressions for the polarization-dependent photometric and ellipsometry quantities become more complex, and analytical expressions for the corresponding "iso-observable" plots become unwieldy, if they can be derived at all.

Regardless of the availability of analytical expressions, such iso-reflectance or "iso-observable"-plots are useful for identifying useful combinations for unambiguous determination of n and k from corresponding spectral data. Clearly, from the single normal incidence reflectance at 40000 cm^{-1}, according to Figure 7, n and k cannot be determined unambiguously. The inclusion of a second measurement would add a further "iso-observable" curve that should result in an intersection with the curves from Figure 7 at the correct pair of n and k [22]. This is exemplified in Figure 8. Here, in addition to the iso-reflectance curves according to (8) (Figures 8a and 8b) and (10) (Figures 8c and 8d), iso-reflectance curves according to (3)-(6) for an incidence angle of 60° are shown.

Note that in Figure 8, regardless of the chosen combination of measurements, there is a certain number of intersection points of the blue and red curves, still defining a set of multiple solutions of the corresponding reverse search task. In Figure 8, the correct solution is again highlighted by a cross. In real characterization practice, however, mathematically correct but physically senseless solutions need to be eliminated to select the physically meaningful solution. As it is seen from Figure 8, it is a proper choice of measurements that is crucial for the identification of the correct solution. In fact, a reliable identification of the correct n- and k-pair can only be expected in the situation highlighted in Figure 8b), corresponding to a combination of normal incidence front reflection with front reflection at 60° at p-polarization. In this situation, although a few discrete intersection points between the blue and red curves exist, the "solutions" corresponding to a small extinction can easily be excluded by an additional transmission measurement. This way the solution marked with the cross may be certainly identified. In other situations, in addition to the intersection points at low extinction, the iso-reflectance curves at normal and oblique incidence are practically coinciding at larger k, providing no chance for the identification of the correct solution.

 doi:10.20944/preprints202604.0015.v1

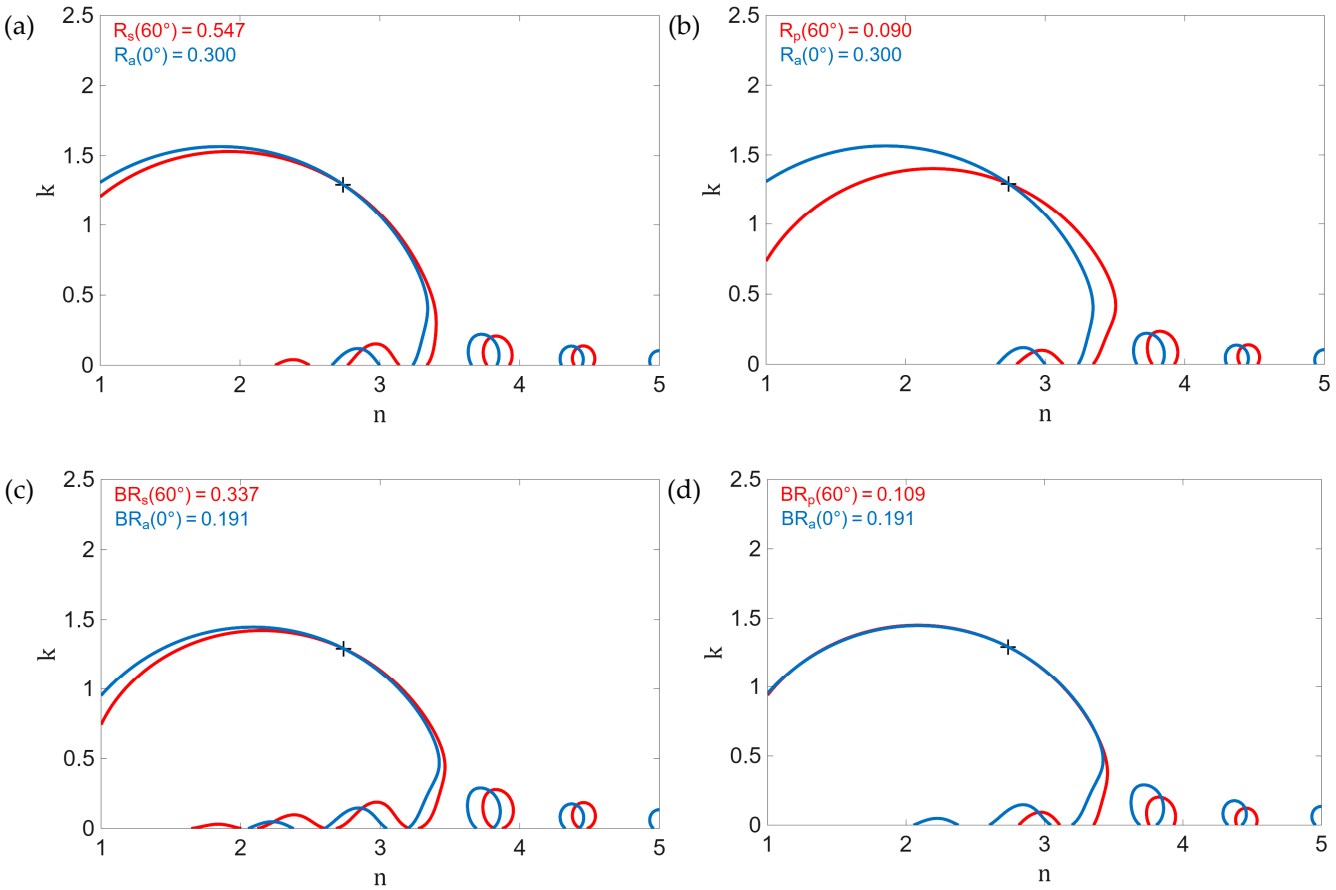

Figure 8. Contour plot for R (a and b) and BR (c and d) for 60° angle of incidence (red line) and normal incidence (blue line); corresponding theoretical values are from a 200 nm Nb_2O_5 single layer coating (optical constants are indicated by a black cross) on a 1 mm thick fused silica substrate at 40000 cm^{-1}.

3. Simulation Results

3.1. Ellipsometry and Photometric Quantities

This section presents "iso-observable" plots of the ellipsometry parameters (Figure 9) and the reflectance for s- and p-polarized light (Figure 10) for nearly perpendicular light incidence (10° angle of incidence) and large angles of incidence (55°, 65°, and 75°) for a 200 nm thick single layer of Nb_2O_5 on a quartz glass substrate (1 mm thickness). The selected range of large angles of incidence is common for ellipsometry and can be also covered by photometry [59–62]. The behavior at the onset of the absorption edge (35000 cm^{-1}) is shown in blue. To illustrate the behavior at higher wavenumbers, a wavenumber of 40000 cm^{-1} was selected as a further example, and the corresponding dependencies are shown in red. The underlying optical constants of Nb_2O_5 are represented by crosses colored accordingly.

The solid lines correspond to the "iso-observable" plots for the exact theoretical value of the respective observable, calculated in terms of (3)-(7). The dotted lines provide information about the error sensitivity. They indicate deviations in optical constants, when tolerances in the measured quantities are assumed. In the graphs, an uncertainty of 0.5° was assumed for Ψ and an uncertainty of 2° for Δ. Thus, the relative uncertainties relative to the possible range of values are the same for both quantities. Clearly, these uncertainties are larger than reported values [63], but more illustrative for the graphical representation. A measurement uncertainty of 0.005 was assumed for the reflectance of both polarizations. Furthermore, iso-transmittance curves corresponding to T= 0.001 are indicated as dashed lines. The respective plots for the discussed simplified model of an infinitely thick Nb_2O_5

 doi:10.20944/preprints202604.0015.v1

layer—i.e., a single interface in measurements from the front side—are represented by thick, semi-transparent lines in the respective color.

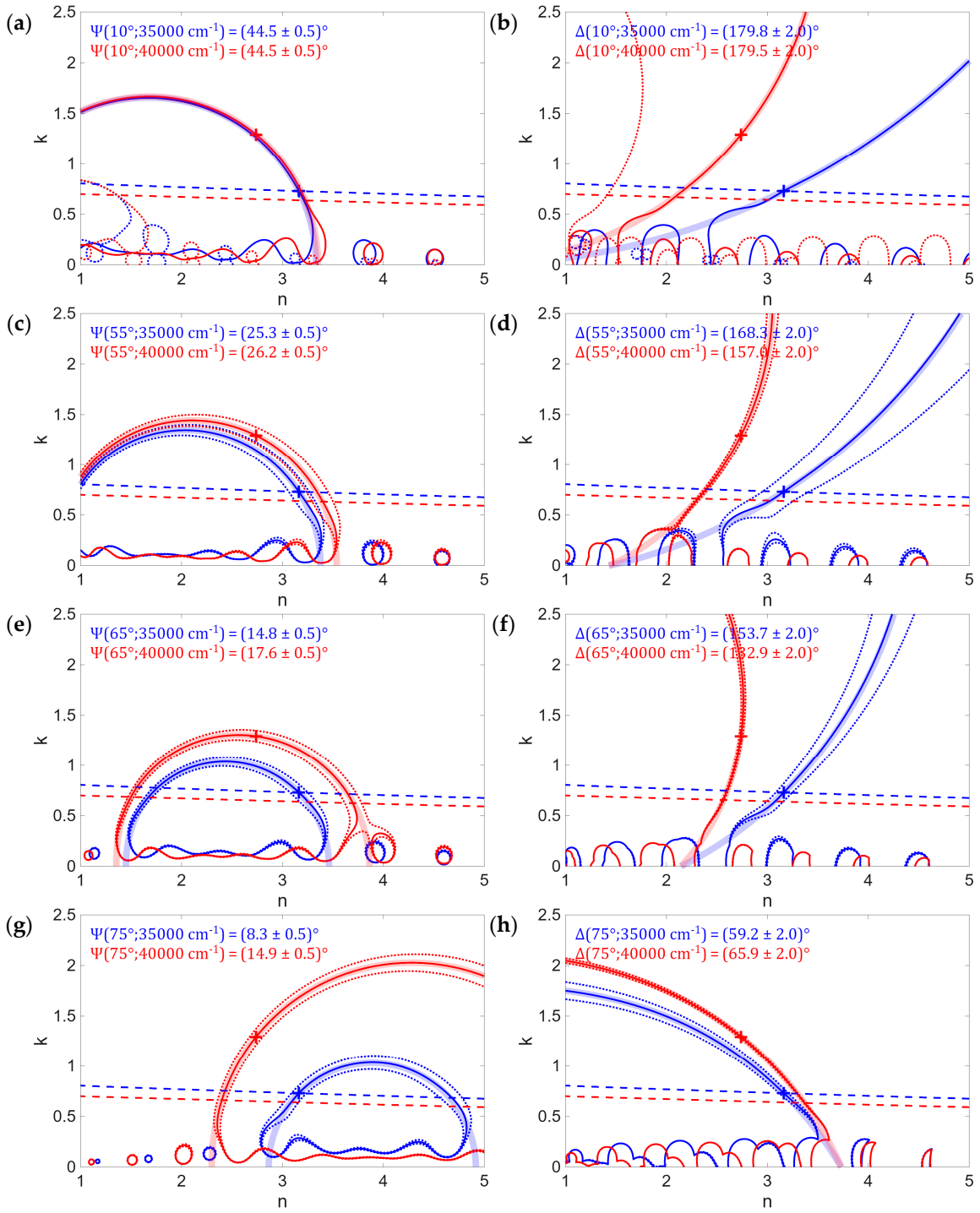

Figure 9. "Iso-observable" (solid lines) of a single layer coating (200 nm Nb_2O_5 on 1 mm fused silica substrate) and a Nb_2O_5-air-interface (thick, semi-transparent lines) for ellipsometry value Ψ (left) and Δ (right) at different angles of incidence (from top to bottom: 10°, 55° 65° and 75°) for different wavenumbers (blue: 35000 cm^{-1}, red: 40000 cm^{-1}). Dotted lines: error sensitivity of the single layer coating for $\Delta\Psi = 0.5°$ and $\Delta\Delta = 2°$. Dashed lines: iso-transmittance for $T = 0.001$. Cross: theoretical optical constants of Nb_2O_5.

 doi:10.20944/preprints202604.0015.v1

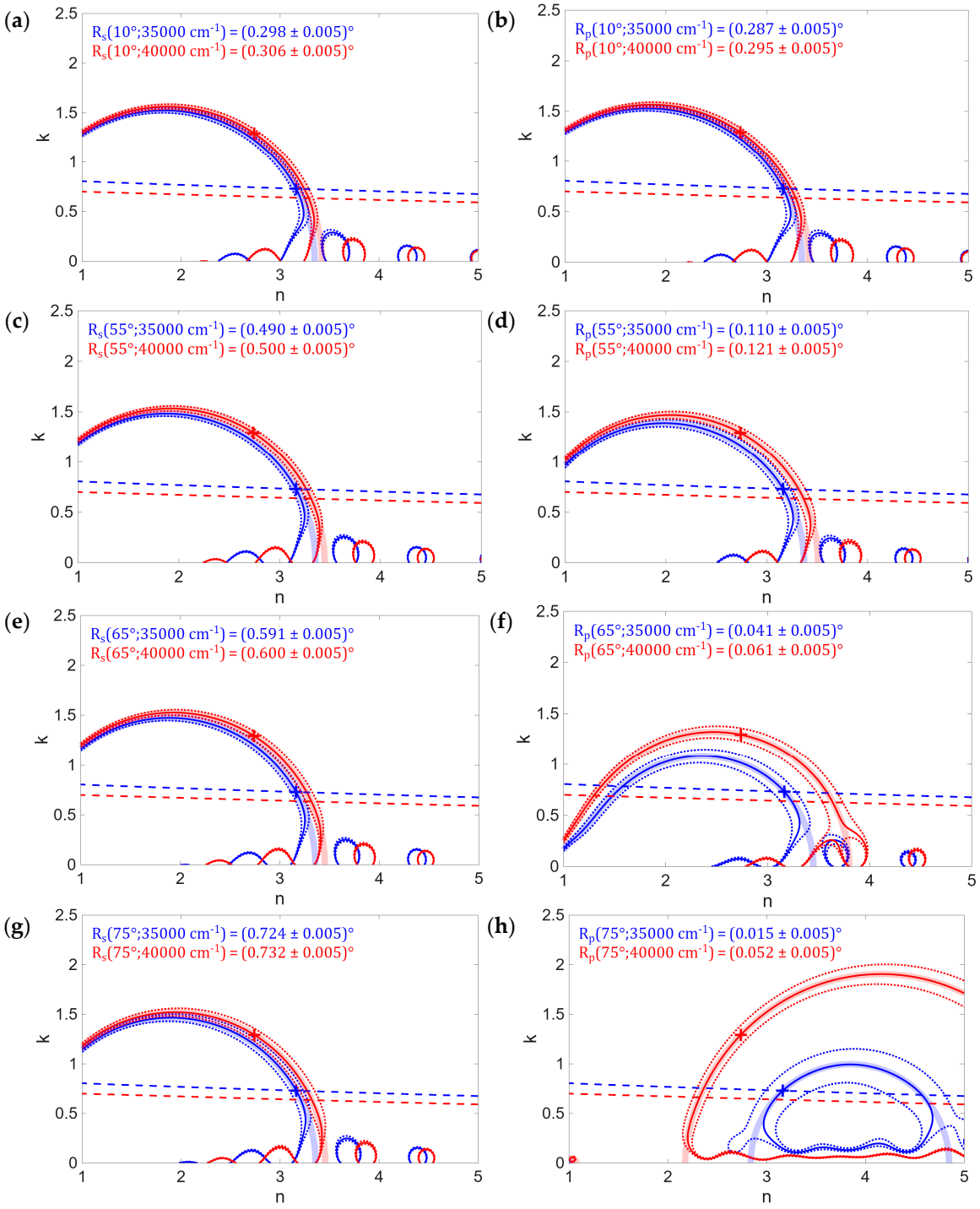

Figure 10. Iso-reflectance (solid lines) of a single layer coating (200 nm Nb_2O_5 on 1 mm fused silica substrate) and a Nb_2O_5-air-interface (thick, semi-transparent lines) for s- (left) and p-polarization (right) at different angles of incidence (from top to bottom: 10°, 55° 65° and 75°) for different wavenumbers (blue: 35000 cm^{-1},red: 40000 cm^{-1}). Dotted lines: error sensitivity of the single layer coating for $\Delta R_s = \Delta R_p = 0.005$. Dashed lines: iso-transmittance for $T = 0.001$. Cross: theoretical optical constants of Nb_2O_5.

Qualitatively, the graphs shown look different from those published in [22]. When comparing with [22], it should be taken into account that [22] addresses the characterization of thin metals films, with thicknesses considerably smaller than the wavelength. Our study is on the analysis of semiconductor films near the absorption edge, with optical thicknesses of the order of the wavelength, which is the basic difference to the systems discussed in [22].

3.2. Merged Discrepancy Functions

 doi:10.20944/preprints202604.0015.v1

Figure 11 shows the discrepancy function for the ellipsometry parameters and for the reflectance (s,p) at the specified angles of incidence. For the discrepancy function, the widely used average root mean square deviation is used [7]. Thereby, a multiplicity of N observables O_i can be considered, while the deviation from the corresponding target value O_i^{target} is weighted according to the tolerance ΔO_i:

$$DF = \left[\frac{1}{N}\sum_{i=1}^{N}\left(\frac{O_i^{\text{target}} - O_i}{\Delta O_i}\right)^2\right]^{1/2} \rightarrow min \tag{11}$$

In this description, mathematical solutions of the reverse search (finding n and k from measured data) are represented by local minima in the DF. When light is incident nearly perpendicularly, the impact of polarization is small, and ellipsometry parameters naturally do not make a significant contribution to finding the correct solution, although the "iso-observable" plots of Ψ and Δ intersect nearly orthogonally (Figure 9). The reason is that the corresponding local minimum (Figure 11a) is very shallow, thus reducing the efficiency of local minimum search algorithms. In combination with other measurements performed at different angles of incidence, they may be helpful for eliminating unphysical multiple solutions observed in the small extinction region. This has a rather transparent physical background. Multiple minima of the discrepancy functions may be caused by interference effects, the latter being strongly dependent on the incidence angle. However, a transmission measurement is clearly superior for ruling out incorrect solutions, since all local minima with k<0.5 can be excluded with a transmission threshold of 0.001 (black dashed line).

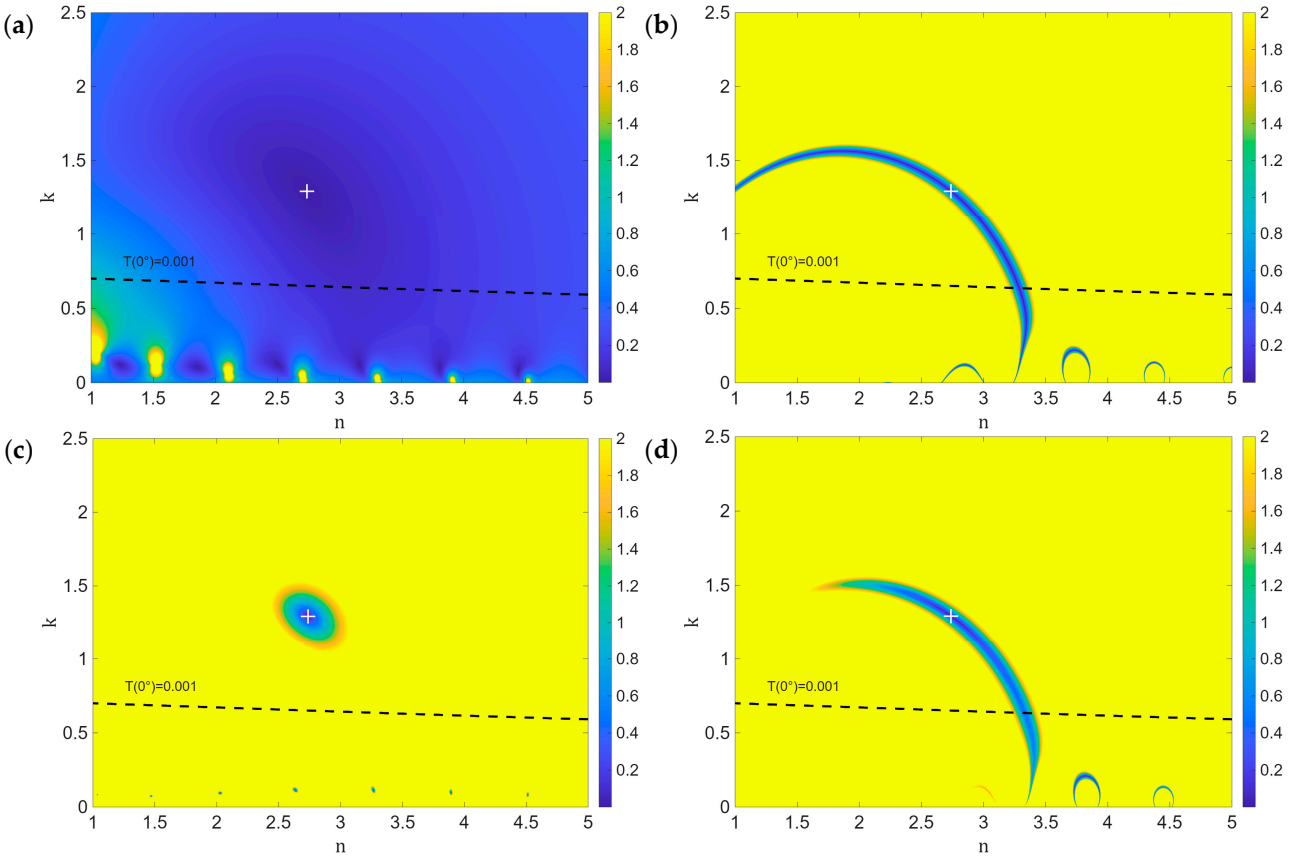

 doi:10.20944/preprints202604.0015.v1

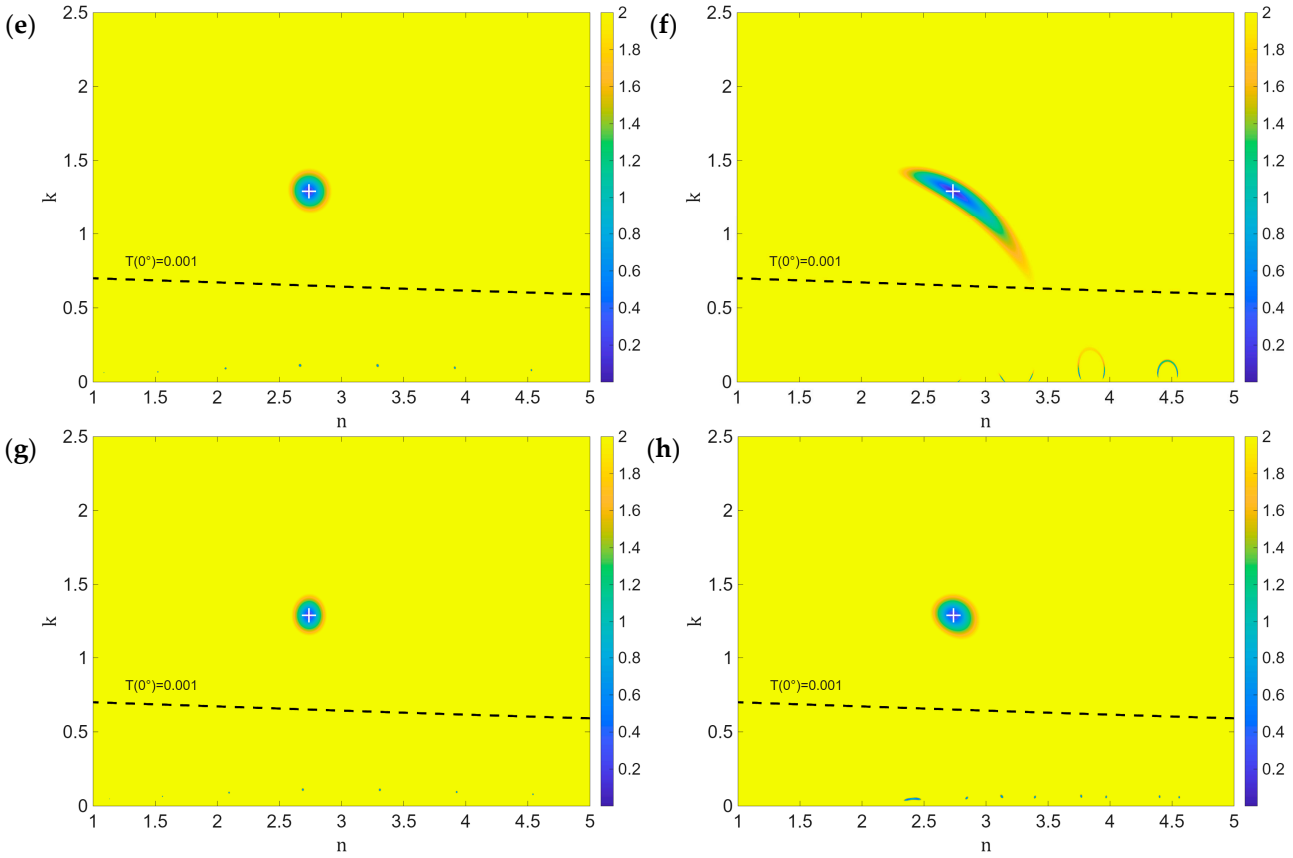

Figure 11. Combined DF for ellipsometry values (left: $O_1 = \Psi$, $O_2 = \Delta$, $\Delta O_1 = 0.5°$, $\Delta O_2 = 2°$) and polarization dependent reflectance (right: $O_1 = R_s$, $O_2 = R_p$, $\Delta O_1 = 0.005$, $\Delta O_2 = 0.005$) for different angles of incidence (from top to bottom: 10°, 55° 65° and 75°).

The local minimum remaining in the ellipsometry parameters coincides with the global minimum in the discussed range of optical constants and, at large angles of incidence, is well-defined by an elliptical region (Figures 11c, 11e and 11g). This is advantageous for local optimization methods. The situation is different for the reflectance. Here, the contours are more crescent-shaped, and many nearly equivalent minima of the discrepancy function correspond to significantly different optical constants. Only at large angles of incidence, the valley in the DF comes close to an elliptic shape (Figure 11h).

When multiple angles of incidence are combined (Figure 12a), combining the angles of incidence 55°, 65° and 75° results in only a slight improvement in the ellipsometry parameters (on left), but eliminates local minima in the region of low extinction coefficients (Figure 12a).

Similarly, a single reflectance measurement at a small incidence angle, combined with a reflectance measurement at an angle of incidence of 75° and p-polarization, can effectively narrow the range of possible solutions. Here, we have numerous local minima in the region of low extinction coefficients (Figure 12d), which can be most efficiently eliminated by performing a transmission measurement with normal light incidence.

 doi:10.20944/preprints202604.0015.v1

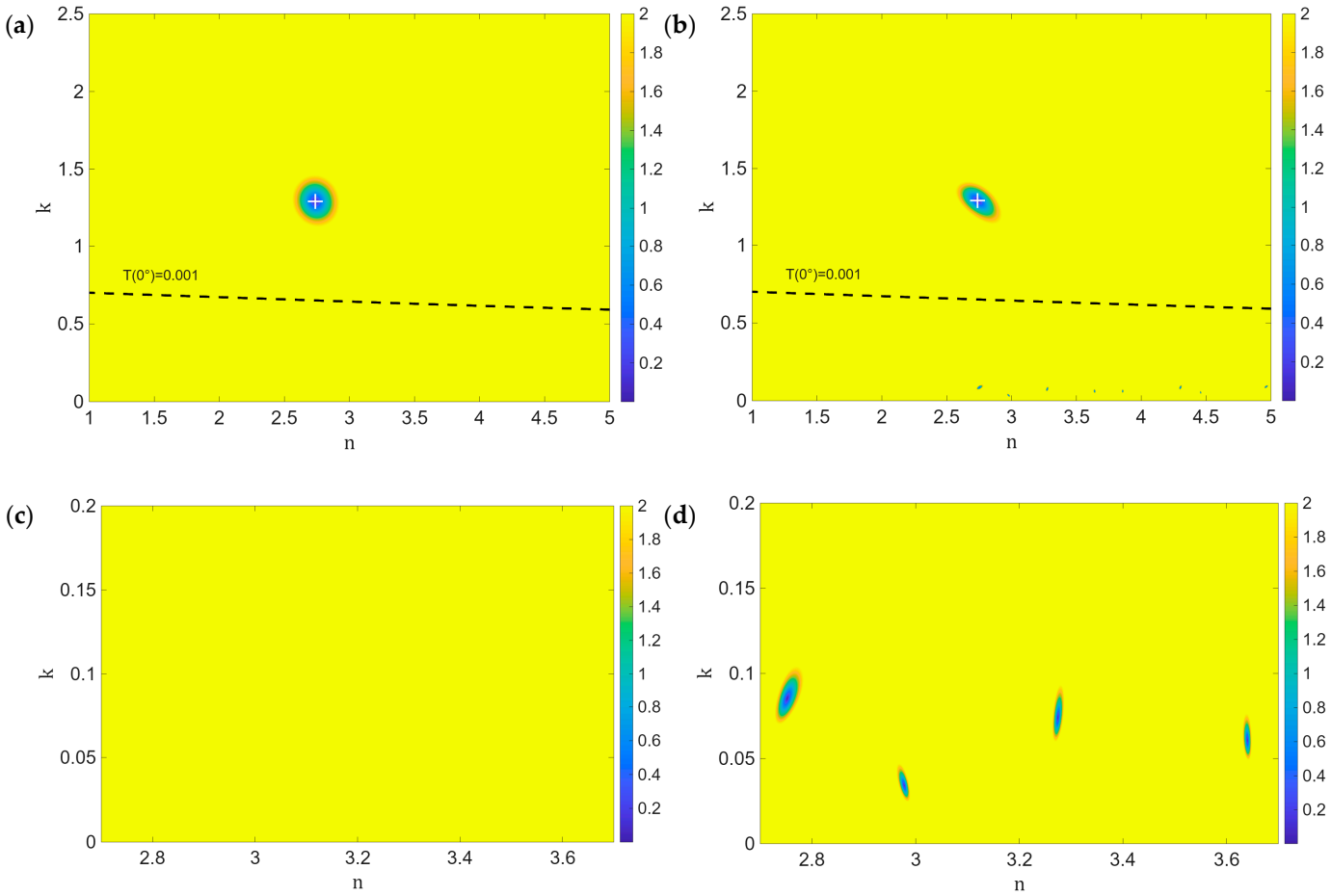

Figure 12. Combined DF for ellipsometry values Ψ and Δ at 55°, 65° and 75° (left) and for R_p at 10° and 75° (right). Bottom: Magnified plot of a region of low extinction coefficients, which potentially contains multiple local minima.

4. Discussion

The "iso-observable" curves presented in section 3.1 provide some guidance for a proper selection for combinations of ellipsometry and photometric quantities for a reliable characterization of single layer coatings at the absorption edge. The application of a combined DF (section 3.2) already demonstrates that the combination of ellipsometry quantities at angle of incidence above 55° results in a well-defined, elliptically shaped local minimum at the correct solution. In the case of polarization dependent reflectance this could be only observed for 75° angle of incidence, in agreement to what has been found in [22,30] for thin metal films. Otherwise, a large, crescent-shaped area is observed, which cannot sufficiently narrow the range of mathematical solutions.

Clearly, the combination of many different measurements can solve this problem [20,64–68] and is essential when more complicated coating models (including multilayer coatings [69–71], inhomogeneities [72–75], anisotropy [76,77], interface roughness [78], photochromic [79] and photoluminescence coatings [80]) are considered. However, in characterization practice, the number of available measurements may be limited by both available measurement time and equipment. When restricting on a combination of two measurements, an identification of the intersection point of the corresponding iso-observable curves will be strongly facilitated when the curves intersect perpendicularly. For two observables O_1 and O_2, this requirement may be quantified in terms of the condition:

 doi:10.20944/preprints202604.0015.v1

$$C_{O_1,O_2} = \left[1 + \frac{\left(\frac{\partial O_1}{\partial n}\right)}{\left(\frac{\partial O_1}{\partial k}\right)}\bigg|_{n_o,k_o} \cdot \frac{\left(\frac{\partial O_2}{\partial n}\right)}{\left(\frac{\partial O_2}{\partial k}\right)}\bigg|_{n_o,k_o}\right]^2 \to 0 \qquad (12)$$

where n_o, k_o represents the correct n-k pair (usually indicated by a cross in the graphs).

The following tables summarize calculated values C_{O_1,O_2} for different choices of the observables in application to the selected Nb_2O_5 model system. Note that a proper selection of observables (reasonable accuracy in n- and k-determination) shall result in a rather small value of C_{O_1,O_2}. On the contrary, when C_{O_1,O_2} becomes large, n is still determined with good accuracy, while the error in k is expected to be very large. The opposite case, namely an accurate determination of k with a large error in n corresponds to a C_{O_1,O_2} value close to 1.

In Table 1 C_{O_1,O_2} is shown for combinations of ellipsometry quantities $\Psi = O_1$ and $\Delta = O_2$. In general, combinations of Ψ and Δ at the same angle of incidence result in a vanishing C_{O_1,O_2} and thus represent a very good choice of measurements (green cells). This is nothing new, but it confirms the validity of criterion (12). Additionally, the combination of Ψ and Δ for 10° and 75° also provides a small value of C_{O_1,O_2}.

Additionally, some combinations appear to be a bad choice for simultaneous n- and k-determination (red cells). This is also true when Δ is recorded at an angle of incidence close to second Brewster angle [33] (here 72.0°). At this angle, R_p/R_s has a minimum, which has direct consequences on the behavior of the ellipsometry parameters (compare (2)). However, the combination of an ellipsometry parameter recorded at φ_{B2} with a parameter recorded at a different angle did not yield any systematic improvement in the parameter C_{O_1,O_2}. Only the combination of both quantities recorded at the second Brewsters angle is useful, because of the obvious orthogonality of the iso-observable plots near the crosses in Figure 13.

Table 1. Numerical values of C_{O_1,O_2} according to (12) for pairs of ellipsometry quantities as observables.

		Δ 10°	Ψ 55°	Δ 55°	Ψ 65°	Δ 65°	Ψ 75°	Δ 75°	Ψ φ_{B2}	Δ φ_{B2}
Ψ	10°	0.000	1.97	0.409	1.23	25.0	0.000	2.74	0.290	5.96
Δ	10°		0.153	12.0	0.696	100.5	6.39	0.000	2.87	1.36
Ψ	55°			0.000	1.14	7.07	0.145	1.96	0.516	3.53
Δ	55°				0.529	250.0	12.3	0.379	4.57	6.53
Ψ	65°					0.000	0.691	1.23	0.853	1.54
Δ	65°						103.6	24.2	26.7	144.4
Ψ	75°							0.000	2.91	1.45
Δ	75°								0.297	5.86
Ψ	φ_{B2}									0.000

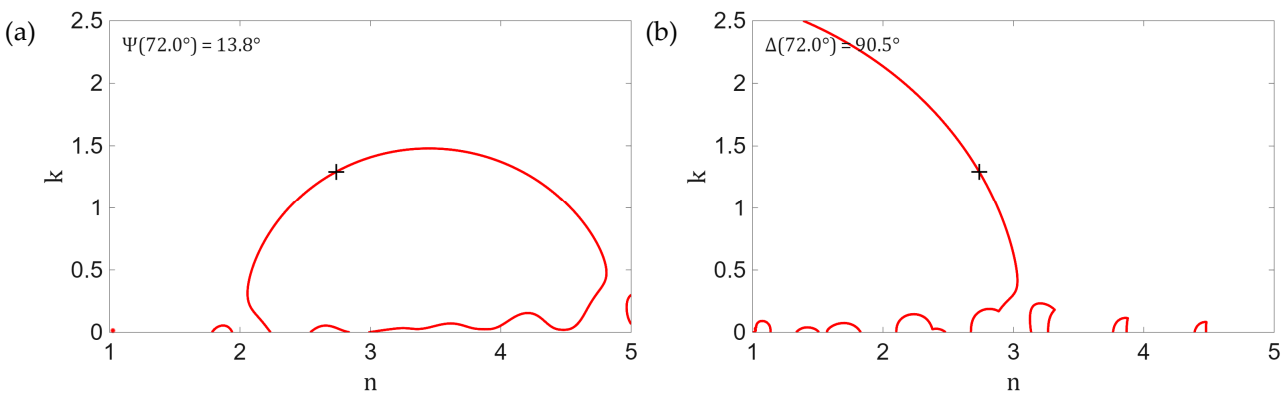

 doi:10.20944/preprints202604.0015.v1

Figure 13. Ellipsometry values Ψ and Δ at second Brewster angle.

In the case of combining $R_s = O_1$ and $R_p = O_2$, we get quite different results for the impact of the angle of incidence (Table 2). Now, the variations in C_{O_1,O_2} are rather small. Very large values ($C_{O_1,O_2} > 10$) are not observed, and C_{O_1,O_2} values for the best choices are still larger than zero. For a good accuracy, the inclusion of R_p at 75° angle of incidence is obviously essential (green fields in Table 2), again in agreement with the situation reported for thin metal films [22,30]. When looking at Figure 10 this becomes instantly clear, because only R_p at 75° angle of incidence shows a significantly different shape in the iso-reflectance plot compared to the corresponding shapes at other angles of incidence. This is clearly related to the key role of the pseudo-Brewster angle [31,32] (here 71.4°). Among the angles investigated in Table 2, it is only the angle of incidence of 75° that exceeds the pseudo-Brewster angle.

Table 2. Numerical values of C_{O_1,O_2} according to (12) for pairs of R_s and R_p.

		R_p	R_s	R_p	R_s	R_p	R_s	R_p	R_s	R_p
	φ	10°	55°		65°		75°		φ_B	
R_s	10°	2.14	2.06	1.87	2.04	1.29	2.02	0.085	2.03	0.553
R_p	10°		2.06	1.87	2.04	1.30	2.03	0.083	2.03	0.551
R_s	55°			1.81	1.97	1.28	1.95	0.112	1.96	0.576
R_p	55°				1.79	1.23	1.78	0.192	1.79	0.635
R_s	65°					1.27	1.93	0.119	1.94	0.582
R_p	65°						1.27	0.623	1.27	0.853
R_s	75°							0.124	1.93	0.586
R_p	75°								0.123	1.94
R_s	φ_B									0.585

Note that, according to Table 2, the combinations of observables favored in Figure 11 (R_s and R_p at 75°) as well as in Figure 12 (R_p at 10° and 75°) clearly belong to the combinations favored in terms of (12).

When combining ellipsometry values and polarization dependent reflectance, the best combination is provided by R_p and Δ if both are recorded at 55° angle of incidence. From the practical point of view, these kinds of combinations are not a good choice because commonly Ψ and Δ are measured together and should be therefore both used for characterization. For this reason, a generalized approach for at least 3 quantities should be applied instead. Note in this context, that the discussion of iso-observable plots may easily be extended to more than 2 observables.

Table 3. Numerical values of C_{O_1,O_2} according to (12) for mixed pairs of observables.

		R_s	R_p	R_s	R_p	R_s	R_p	R_s	R_p	R_s	R_p
	φ	10°		55°		65°		75°		φ_B	
Ψ	10°	2.42	2.42	2.31	2.07	2.29	1.36	2.27	0.023	2.28	0.480
Δ		0.028	0.027	0.047	0.115	0.053	0.57	0.057	5.18	0.055	2.14
Ψ	55°	1.79	1.79	1.74	1.61	1.72	1.21	1.71	0.233	1.72	0.660
Δ		0.135	0.140	0.081	0.007	0.070	0.35	0.063	9.58	0.065	3.09
Ψ	65°	1.19	1.19	1.18	1.15	1.18	1.06	1.18	0.738	1.18	0.900
Δ		16.0	16.2	13.7	8.839	13.2	0.240	12.8	75.2	12.9	14.3
Ψ	75°	0.023	0.022	0.042	0.107	0.047	0.559	0.051	5.28	0.050	2.16
Δ		2.39	2.40	2.29	2.05	2.27	1.35	2.25	0.027	2.25	0.486
Ψ	φ_{B2}	0.378	0.376	0.407	0.482	0.415	0.784	0.420	2.53	0.418	1.47
Δ		4.85	4.87	4.53	3.82	4.46	1.84	4.40	0.708	4.42	0.111

 doi:10.20944/preprints202604.0015.v1

Hence, criterion (12) appears to be useful for identifying possible combinations of measurements for reliable determination of n and k from absorbing thin solid films. The essence of the idea behind (12) is to guarantee a rather symmetrical shape of the minimum of the discrepancy function (11). Note that (12) does not provide information on the steepness of the minimum. This is evident from Table 1, where the combination of ellipsometry parameters at 10° clearly minimizes (12), although it is clear from Figure 11 left on top, that the minimum is although symmetric, but too shallow for reliable n-k -determination. Therefore, (12) has to be regarded as a necessary condition for a proper choice of measurements, but it is not sufficient. After having got a first characterization result from an arbitrarily chosen measurement, (12) may be useful in practice for excluding measurements that are improper for enhancing the accuracy in a refined n-k-determination procedure.

5. Conclusions

In this study, we addressed the choice of measurements applicable for unambiguous determination of the optical constants n and k of a strongly absorbing thin solid film in a rather limited spectral range. We explicitly addressed the case when the optical film thickness is comparable to or even larger than the wavelength of the incident light. Because of the very small transmittance, emphasis was placed on combing ellipsometry as well as reflectance measurements at different angles of incidence. In order to reduce measurement time and effort, the focus was on the combination of two measurements, although a generalization of the applied strategy to more than 2 measurements is possible.

Similarly to what has been reported earlier for ultrathin metal films [22], the method of iso-observable plots in the n-k-plane provides an illustrative insight into the arrangement of multiple solutions of the n-k-determination in a practical characterization task. For the particular case of two measurements, we provided a necessary (not sufficient) criterion for the choice of measurements favored for an unambiguous n-k-determination. The criterion makes use of the parameter C_{O_1,O_2} as defined in (12) and is related to the shape of the minimum in the discrepancy function in the n-k-plane as summarized in Table 4:

Table 4. Important values of C_{O_1,O_2}.

C_{O_1,O_2}	Δn	Δk
0	Reasonable compromise	
1	large	small
$\rightarrow \infty$	Small	large

Depending on the required information, different C_{O_1,O_2}, and correspondingly different combinations of measurements may be favored.

Practical simulations concerned the model system of a 200 nm thick Nb_2O_5 film in the region of the fundamental absorption edge. The simulations reproduced the well-known result that ellipsometry provides a reliable tool for n- and k-determination of thin solid films (green fields in the diagonal of Table 1). Nevertheless, alternative suitable combinations of measurements could be identified, too. Among them we note the combination of near-normal incidence reflectance with the reflectance of p-polarized light at 75° incidence angle. We also have to state that from the simulations performed in this study (tabs.1-3), no simple rule of thumb for a proper combination of observables and incidence angles could be identified. It is our point of view that this enhances the value of criterion (12), which can easily be applied to any combination of measurement set-ups available in the corresponding lab.

 doi:10.20944/preprints202604.0015.v1

In all situations, the inclusion of a transmittance signal (particularly when it is very small) may nevertheless be useful for excluding multiple solutions corresponding to small extinction values.

Author Contributions: Conceptualization, S.W. and O.S.; methodology, S.W. and O.S.; software, S.W.; validation, S.W. and O.S.; formal analysis, S.W. and O.S.; investigation, S.W. and O.S.; resources, S.W. and O.S.; data curation, S.W. and O.S.; writing—original draft preparation, S.W. and O.S.; writing—review and editing, O.S. and S.W.; visualization, S.W. and O.S.; supervision, S.W. and O.S.; project administration, S.W.; funding acquisition, S.W. and O.S. All authors have read and agreed to the published version of the manuscript.

Funding: This research was funded by Fraunhofer Gesellschaft, grant number 601001.

Data Availability Statement: No data available.

Conflicts of Interest: The authors declare no conflicts of interest.

References

1. Stenzel, O.; Wilbrandt, S.; Kaiser, N.; Vinnichenko, M.; Munnik, F.; Kolitsch, A.; Chuvilin, A.; Kaiser, U.; Ebert, J.; Jakobs, S.; Kaless, A.; Wüthrich, S.; Treichel, O.; Wunderlich, B.; Bitzer, M. and Grössl M. The correlation between mechanical stress, thermal shift and refractive index in HfO2, Nb2O5, Ta2O5 and SiO2 layers and its relation to the layer porosity. *Thin Solid Films* **2009,** *517,* 6058–6068, 10.1016/j.tsf.2009.05.009.
2. Targove, J.D.; Macleod, H.A. Verification of momentum transfer as the dominant densifying mechanism in ion-assisted deposition, *Appl. Opt.* **1988**, 27, 3779–3781, https://doi.org/10.1364/AO.27.003779.
3. Davis, C.A. A simple model for the formation of compressive stress in thin films by ion bombardment. Thin Solid Films **1993**, 226, 30–34; https://doi.org/10.1016/0040-6090(93)90201-Y.
4. Ehlers, H.; Becker, K.-J.; Beckmann, R.; Beermann, N.; Brauneck, U.; Fuhrberg, P.; Gaebler, D.; Jakobs, S.; Kaiser, N.; Kennedy, M.; Koenig, F.; Laux, S.; Mueller, J. C.; Rau, B.; Riggers, W.; Ristau, D.; Schaefer, D. and Stenzel, O. Ion-assisted deposition processes: industrial network IntIon, In: Proc. SPIE 5250, 2004, Advances in Optical Thin Films; https://doi.org/10.1117/12.514817.
5. Harhausen, J.; Foest, R.; Stenzel, O.; Wilbrandt, S.; Franke, C. and Brinkmann, R. Concepts for in situ characterization and control of plasma ion assisted deposition processes. *Thin Solid Films* **2019,** *673,* 94–103, 10.1016/j.tsf.2019.01.038.
6. Pulker, H. K. Characterization of optical thin films. *Appl. Opt.* **1979,** *18,* 1969–1977, 10.1364/AO.18.001969.
7. Dobrowolski, J. A.; Ho, F. C. and Waldorf, A. Determination of optical constants of thin film coating materials based on inverse synthesis. *Applied Optics* **1983,** *22,* 3191, 10.1364/ao.22.003191.
8. Tikhonravov, A. V.; Amotchkina, T. V.; Trubetskov, M. K.; Francis, R. J.; Janicki, V.; Sancho-Parramon, J.; Zorc, H. and Pervak, V. Optical characterization and reverse engineering based on multiangle spectroscopy. *Appl. Opt.* **2012,** *51,* 245–254, 10.1364/AO.51.000245.
9. Woollam, J. A.; Hilfiker, J. N. and Synowicki, R. A. Ellipsometry, variable angle spectroscopic. In Wiley Encyclopedia of Electrical and Electronics Engineering, ed. by J. Webster, Wiley, 2000; https://doi.org/10.1002/047134608X.W4039.pub2.
10. Tikhonravov, A., Trubetskov, M., Amotchkina, T., Tikhonravov, A., Ristau, D. and Günster, S., Reliable determination of wavelength dependence of thin film refractive index. In: SPIE International Society for Optics and Photonics, 2003, 331–342; https://doi.org/10.1117/12.505554.
11. Tikhonravov, A. V.; Amotchkina, T. V.; Trubetskov, M. K.; Francis, R. J.; Janicki, V.; Sancho-Parramon, J.; Zorc, H. and Pervak, V. Optical characterization and reverse engineering based on multiangle spectroscopy. Appl. Opt. 2012, 51, 245–254, 10.1364/AO.51.000245.
12. Gao, L.; Lemarchand, F. and Lequime, M. Exploitation of multiple incidences spectrometric measurements for thin film reverse engineering. *Opt. Express* **2012**, 20, 15734–15751, 10.1364/OE.20.015734.
13. Kozlova, N. S.; Levashov, E. A.; Kiryukhantsev-Korneev, P. V.; Sytchenko, A. D. and Zabelina, E. V. The possibilities of multi-angle spectrophotometry for determining the parameters of films on single-layer structures. *Izvestiya Vysshikh Uchebnykh Zavedenii. Materialy Elektronnoi Tekhniki = Materials of Electronics Engineering* **2022,** *25,* 154–163, 10.17073/1609-3577-2022-2-154-163.

 doi:10.20944/preprints202604.0015.v1

14. Larruquert, J. I.; Aznárez, J. A.; Méndez, J. A.; Malvezzi, A. M.; Poletto, L. and Covini, S. Optical properties of scandium films in the far and the extreme ultraviolet. *Appl. Opt.* **2004,** *43,* 3271–3278, 10.1364/AO.43.003271.
15. Rey-Bayle, M.; Bendoula, R.; Caillol, N. and Roger, J.-M. Multiangle near infrared spectroscopy associated with common components and specific weights analysis for in line monitoring. *Journal of Near Infrared Spectroscopy* **2019,** *27,* 134-146, 10.1177/0967033519830062.
16. Wagner, T.; Hilfiker, J.; Tiwald, T.; Bungay, C. and Zollner, S. Materials Characterization in the Vacuum Ultraviolet with Variable Angle Spectroscopic Ellipsometry. *physica status solidi (a)* **2001,** *188,* 1553-1562, https://doi.org/10.1002/1521-396X(200112)188:4<1553::AID-PSSA1553>3.0.CO;2-A.
17. Born, M.; Wolf, E. *Principles of Optics*; Pergamon Press: Oxford, UK; London, UK; Edinburgh, UK; New York, NY, USA; Paris, France; Frankfurt, Germany, 1968.
18. Amotchkina, T. V.; Trubetskov, M. K.; Tikhonravov, A. V.; Janicki, V.; Sancho-Parramon, J. and Zorc, H. Comparison of two techniques for reliable characterization of thin metal–dielectric films. *Appl. Opt.* **2011,** *50,* 6189–6197, 10.1364/AO.50.006189.
19. Stenzel, O. *The Physics of Thin Film Optical Spectra: An Introduction;* Springer International Publishing, 2024.
20. Franta, D.; Hroncová, B.; Dvořák, J.; Vohánka, J.; Franta, P.; Ohlídal, I.; Pekař, V. and Škoda, D. Wide spectral range optical characterization of niobium pentoxide (Nb2O5) films by universal dispersion model. *Optical Materials* **2024,** *157,* 116133, https://doi.org/10.1016/j.optmat.2024.116133.
21. Larruquert, J. I. Characterization of the optical constants of materials from the visible to the soft x-rays. In: SPIE International Society for Optics and Photonics, 2008, 71010W.
22. Nestell, J. E. and Christy, R. W. Derivation of Optical Constants of Metals from Thin-Film Measurements at Oblique Incidence. *Appl. Opt.* **1972,** *11,* 643–651, 10.1364/AO.11.000643.
23. Elizalde, E. and Rueda, F. On the determination of the optical constants n(λ) and α(λ) of thin supported films. *Thin Solid Films* **1984,** *122,* 45-57, https://doi.org/10.1016/0040-6090(84)90377-8.
24. Elizalde, E.; Frigerio, J. M. and Rivory, J. Determination of thickness and optical constants of thin films from photometric and ellipsometric measurements. *Appl. Opt.* **1986,** *25,* 4557–4561, 10.1364/AO.25.004557.
25. Ohlídal, I. and Navrátil, K. Simple method of spectroscopic reflectometry for the complete optical analysis of weakly absorbing thin films: Application to silicon films. *Thin Solid Films* **1988,** *156,* 181-190, https://doi.org/10.1016/0040-6090(88)90313-6.
26. Kozlova, N. S.; Shayapov, V. R.; Zabelina, E. V.; Kozlova, A. P.; Zhukov, R. N.; Kiselev, D. A.; Malinkovich, M. D. and Voronova, M. I. Spectrophotometric determination of optical parameters of lithium niobate films. *Modern Electronic Materials* **2017,** *3,* 122-126, https://doi.org/10.1016/j.moem.2017.09.001.
27. Gushterova, P. and Sharlandjiev, P. Determination of optical constants (n, k, d) of very thin films deposited on absorbing substrate. *Vacuum* **2004,** *76,* 185-189, https://doi.org/10.1016/j.vacuum.2004.07.009.
28. Gallardo, J.; Durán, A.; Di Martino, D. and Almeida, R. Structure of inorganic and hybrid SiO2 sol–gel coatings studied by variable incidence infrared spectroscopy. *Journal of Non-Crystalline Solids* **2002,** *298,* 219-225, https://doi.org/10.1016/S0022-3093(02)00921-3.
29. Gaballah, A.; Nicolosi, P.; Ahmed, N.; Jimenez, K.; Pettinari, G.; Gerardino, A. and Zuppella, P. Vacuum ultraviolet quarter wave plates based on SnTe/Al bilayer: Design, fabrication, optical and ellipsometric characterization. *Applied Surface Science* **2019,** *463,* 75-81, https://doi.org/10.1016/j.apsusc.2018.08.190.
30. Babeva, T. and Kitova, S. Reflectance methods for determining the optical constants of highly absorbing films: comparative analysis of the accuracy. *Journal of Optics A: Pure and Applied Optics* **2007,** *9,* 145-151, 10.1088/1464-4258/9/2/004.
31. Azzam, R. M. A. and Ugbo, E. E. Contours of constant pseudo-Brewster angle in the complex $\in$ plane and an analytical method for the determination of optical constants. *Applied Optics* **1989,** *28,* 5222-5228, 10.1364/AO.28.005222.
32. Kim, S. Y. and Vedam, K. Analytic solution of the pseudo-Brewster angle. *Journal of the Optical Society of America A* **1986,** *3,* 1772-1773, 10.1364/JOSAA.3.001772.
33. Azzam, R. M. A. Explicit equations for the second Brewster angle of an interface between a transparent and an absorbing medium. *J. Opt. Soc. Am.* **1983**, 73, 1211–1212, 10.1364/JOSA.73.001211.

 doi:10.20944/preprints202604.0015.v1

34. Alsamman, A. and Azzam, R. M. A. Difference between the second-Brewster and pseudo-Brewster angles when polarized light is reflected at a dielectric–conductor interface. *Journal of the Optical Society of America A* **2010,** *27,* 1156-1161, 10.1364/JOSAA.27.001156.
35. Potter, P. Reflectometer for pseudo-Brewster angle spectrometry (BAIRS). In: Proc. SPIE 4103, Optical Diagnostic Methods for Inorganic Materials II, 2000, 85-89; https://doi.org/10.1117/12.403574.
36. Ogusu, K.; Suzuki, K. and Nishio, H. Simple and accurate measurement of the absorption coefficient of an absorbing plate by use of the Brewster angle. *Optics Letters* **2006,** *31,* 909-911, 10.1364/OL.31.000909.
37. Regalado, L. E.; Machorro, R.; Leyva-Lucero, M. and Garcia-Llamas, R. Angle scanning reflectometry: study of two characteristic isoreflectance angles. *Journal of Physics D: Applied Physics* **1992,** *25,* 1365-1370, 10.1088/0022-3727/25/9/015.
38. Humphreys-Owen, S. P. F. Comparison of Reflection Methods for Measuring Optical Constants without Polarimetric Analysis, and Proposal for New Methods based on the Brewster Angle. *Proceedings of the Physical Society* **1961,** *77,* 949, 10.1088/0370-1328/77/5/301.
39. Bhattacharyya, S.; Gayen, R.; Paul, R. and Pal, A. Determination of optical constants of thin films from transmittance trace. *Thin Solid Films* **2009,** *517,* 5530-5536, https://doi.org/10.1016/j.tsf.2009.03.168.
40. Swanepoel, R. Determination of the thickness and optical constants of amorphous silicon. *Journal of Physics E: Scientific Instruments* **1983,** *16,* 1214–1222, 10.1088/0022-3735/16/12/023.
41. Edmund Optics, Understanding Neutral Density Filters, Available online: https://www.edmundoptics.com/knowledge-center/application-notes/optics/understanding-neutral-density-filters (accessed on 31.03.2026)
42. Padera, F., High Absorbance Scanning with LAMBDA 850+ and 1050+ Spectrophotometers; Available online: https://www.perkinelmer.com/library/app-high-absorbance-scanning-with-lambda-850-and-1050-spectrophotometers.html (accessed on 31.03.2026)
43. Franta, D.; Vohánka, J.; Dvořák, J.; Franta, P.; Ohlídal, I.; Klapetek, P.; Březina, J. and Škoda, D. Wide spectral range optical characterization of tantalum pentoxide (Ta2O5) films by the universal dispersion model. *Opt. Mater. Express* **2025,** *15,* 903–919, 10.1364/OME.550708.
44. Franta, D.; Nečas, D.; Ohlídal, I. and Giglia, A. Optical characterization of SiO2 thin films using universal dispersion model over wide spectral range.In: SPIE International Society for Optics and Photonics, 2016, 989014.
45. Franta, D.; Dubroka, A.; Wang, C.; Giglia, A.; Vohánka, J.; Franta, P. and Ohlídal, I. Temperature-dependent dispersion model of float zone crystalline silicon. *Applied Surface Science* **2017,** *421,* 405-419, https://doi.org/10.1016/j.apsusc.2017.02.021.
46. Stenzel, O.; Wilbrandt, S. Some Basic Considerations on the Reflectance of Smooth Metal Surfaces: Fresnel's Formula and More. *Coatings* **2026**, *16*, 236. https://doi.org/10.3390/coatings16020236.
47. Fujiwara, H. *Spectroscopic Ellipsometry: Principles and Applications*; John Wiley & Sons: Hoboken, NJ, USA, 2007.
48. Nozières, P. and Pines, D. Electron Interaction in Solids. Characteristic Energy Loss Spectrum. *Phys. Rev.* **1959,** *113,* 1254–1267, 10.1103/PhysRev.113.1254.
49. Lucarini, V.; Bassani, F.; Peiponen, K. E. and Saarinen, J. J. Dispersion theory and sum rules in linear and nonlinear optics. *La Rivista del Nuovo Cimento* **2003,** *26,* 1–120, 10.1393/ncr/i2003-10006-x.
50. Franta, D.; Nečas, D.; Zajíčková, L.; Ohlídal, I.; Stuchlík, J. and Chvostová, D. Application of sum rule to the dispersion model of hydrogenated amorphous silicon. *Thin Solid Films* **2013,** *539,* 233–244, 10.1016/j.tsf.2013.04.012.
51. Arndt, D.P.; Azzam, R.M.A.; Bennett, J.M.; Borgogno, J.P.; Carniglia, C.K.; Case, W.E.; Dobrowolski, J.A.; Gibson, U.J.; Hart, T.T.; Ho, F.C.; et al. Multiple determination of the optical constants of thin-film coating materials. Appl. Opt. **1984**, 23, 3571–3596; https://doi.org/10.1364/AO.23.003571.
52. Bosch, S.; Monzonis, F. General inversion method for single-wavelength ellipsometry of samples with an arbitrary number of layers. *J. Opt. Soc. Am. A* **1995**, *12*, 1375–1379.
53. Macleod, A. Phase Matters, *SPIE's OE magazine*, June/July (2005), pp. 29-31.
54. Holl, H. B. Specular Reflection and Characteristics of Reflected Light*. *J. Opt. Soc. Am.* **1967,** *57,* 683–690, 10.1364/JOSA.57.000683.

 doi:10.20944/preprints202604.0015.v1

55. Azzam, R. M. A. and Zaghloul, A.-R. M. Principal angle, principal azimuth, and principal-angle ellipsometry of film-substrate systems. *J. Opt. Soc. Am.* **1977,** *67,* 1058–1065, 10.1364/JOSA.67.001058.
56. Cojocaru, E. Contours of the constant third Brewster angle in the complex plane of a dielectric constant. *Applied Optics* **1995,** *34,* 7864-7869, 10.1364/AO.34.007864.
57. Zaghloul, A.-R. M. and Azzam, R. M. A. Constant-psi constant-delta contour maps: applications to ellipsometry and to reflection-type optical devices. *Appl. Opt.* **1982,** *21,* 739–743, 10.1364/AO.21.000739.
58. Ohlídal, I.; Franta, D.; Ohlídal, M. and Navrátil, K. Optical characterization of nonabsorbing and weakly absorbing thin films with the wavelengths related to extrema in spectral reflectances. *Appl. Opt.* **2001,** *40,* 5711–5717, 10.1364/AO.40.005711.
59. van Nijnatten, P. Optical analysis of coatings by variable angle spectrophotometry. *Thin Solid Films* **2008,** *516,* 4553-4557, https://doi.org/10.1016/j.tsf.2007.06.027.
60. van Nijnatten, P. An automated directional reflectance/transmittance analyser for coating analysis. *Thin Solid Films* **2003,** *442,* 74-79, https://doi.org/10.1016/S0040-6090(03)00947-7.
61. Burt, T. C.; Comerford, J.; Bricker, C.; Hind, A. and Death, D. L. Automated multi-point analysis with multi-angle photometric spectroscopy.In: SPIE International Society for Optics and Photonics, 2014, 89920H.
62. Nevas, S.; Manoocheri, F.; Ikonen, E.; Tikhonravov, A. V.; Kokarev, M. A. and Trubetskov, M. K. Optical metrology of thin films using high-accuracy spectrophotometric measurements with oblique angles of incidence. In: SPIE International Society for Optics and Photonics, 2004, 234 – 242.
63. Kostruba, A. M. and Vlokh, O. G. Accuracy of traditional ellipsometry and complex ellipsometry-transmission photometry techniques for absorptive-film/transparent-substrate systems. In: SPIE International Society for Optics and Photonics, 1997, 266 – 271.
64. Lamminpää, A.; Nevas, S.; Manoocheri, F. and Ikonen, E. Characterization of thin films based on reflectance and transmittance measurements at oblique angles of incidence. *Appl. Opt.* **2006,** *45,* 1392–1396, 10.1364/AO.45.001392.
65. Xie, A.; Nian, S.; Zheng, Y.; Liu, S.; Dai, B.; Lu, Q.; Jin, Y. and Shao, J. High-precision film thickness detection method based on multi-angle spectroscopy and LSTM. In: SPIE International Society for Optics and Photonics, 2025, 137201K.
66. Tyson, J. J.; Rahman, T. and Boden, S. A. Angle-Resolved Spectrophotometry for the Optical Characterization of Material Surfaces. *IEEE Transactions on Instrumentation and Measurement* **2022,** *71,* 1–8, 10.1109/TIM.2022.3146947.
67. Shaaban, E.; El-Hagary, M.; Emam-Ismail, M.; Abd Elnaeim, A.; Moustafa, S. and Adel, A. Optical characterization of polycrystalline ZnSe1−xTex thin films using variable angle spectroscopic ellipsometry and spectrophotmetery techniques. *Materials Science in Semiconductor Processing* **2015,** *39,* 735-741, https://doi.org/10.1016/j.mssp.2015.06.048.
68. Franta, D.; Necas, D.; Ohlidal, I.; Hrdlicka, M.; Pavlista, M.; Frumar, M. and Ohlidal, M. Combined method of spectroscopic ellipsometry and photometry as an efficient tool for the optical characterisation of chalcogenide thin films. *Journal of Optoelectronics and Advanced Materials* **2009,** *11,* 1891-1898.
69. Gao, L.; Lemarchand, F. and Lequime, M. Refractive index determination of SiO2 layer in the UV/Vis/NIR range: spectrophotometric reverse engineering on single and bi-layer designs. *J. Eur. Opt. Soc.-Rapid Publ.* **2013,** *8,* 13010, 10.2971/jeos.2013.13010.
70. Law, A. M.; Isherwood, P. J. M.; Walls, J. M.; Tyson, J. J.; Cao, C. and Boden, S. A. Variable Angle Reflectance Measurements of Anti-Reflection Coatings on Glass.In: IEEE 2024, 1056-1060.
71. Likhachev, D. Efficient thin-film stack characterization using parametric sensitivity analysis for spectroscopic ellipsometry in semiconductor device fabrication. *Thin Solid Films* **2015,** *589,* 258-263, https://doi.org/10.1016/j.tsf.2015.05.049.
72. Sotsky, A. B.; Krivetskii, K. N.; Parashkov, S. O. and Sotskaya, L. I. Lorentz-Lorenz Model for the Inverse Problem of Inhomogeneous Layer Spectrometry. *Journal of Applied Spectroscopy* **2016,** *83,* 845–853, 10.1007/s10812-016-0373-3.
73. Anisimov, A. V. and Sh Khasanov, I. Algorithm for optical characterization of dielectric gradient index nanofilm by surface plasmon resonance spectroscopy. *Journal of Physics: Conference Series* **2021,** *2091,* 012067, 10.1088/1742-6596/2091/1/012067.

 doi:10.20944/preprints202604.0015.v1

74. Russev, S. C.; Tsutsumanova, G. G.; Stefanov, I. L. and Hadjichristov, G. B. Ellipsometrical characterization of complex refractive index depth profile of 50 keV silicon ion implanted PMMA. *Vacuum* **2013,** *94,* 19-25, https://doi.org/10.1016/j.vacuum.2013.01.014.
75. Dvořák, J.; Vohánka, J.; Buršíková, V.; Franta, D. and Ohlídal, I. Optical Characterization of Inhomogeneous Thin Films Deposited onto Non-Absorbing Substrates. *Coatings* **2023,** *13,* 873, 10.3390/coatings13050873.
76. Pettersson, L.; Johansson, T.; Carlsson, F.; Arwin, H. and Inganäs, O. Anisotropic optical properties of doped poly(3,4-ethylenedioxythiophene). *Synthetic Metals* **1999,** *101,* 198-199, https://doi.org/10.1016/S0379-6779(98)01215-6.
77. Franta, D.; Nečas, D. and Ohlídal, I. Anisotropy-enhanced depolarization on transparent film/substrate system. *Thin Solid Films* **2011,** *519,* 2637-2640, https://doi.org/10.1016/j.tsf.2010.12.113.
78. Franta, D.; Ohlídal, I.; Nečas, D.; Vižd'a, F.; Caha, O.; Hasoň, M. and Pokorný, P. Optical characterization of HfO2 thin films. *Thin Solid Films* **2011,** *519,* 6085-6091, https://doi.org/10.1016/j.tsf.2011.03.128.
79. Montero, J. and Karazhanov, S. Z. Spectroscopic Ellipsometry and Microstructure Characterization of Photochromic Oxygen-Containing Yttrium Hydride Thin Films. *physica status solidi (a)* **2018,** *215,* 1701039, https://doi.org/10.1002/pssa.201701039.
80. Horcholle, B. Growth and study of Tb3+ doped Nb2O5 thin films by radiofrequency magnetron sputtering: Photoluminescence properties. *Applied Surface Science* **2022,** *597,* 153711, https://doi.org/10.1016/j.apsusc.2022.153711.